Invited Paper https://doi.org/10.7733/jnfcwt.2019.17.2.127

Effect of AlF_3 on Zr Electrorefining Process in Chloride-Fluoride Mixed Salts for the Treatment of Cladding Hull Wastes

폐 피복관 처리를 위한 염소계-불소계 혼합용융염 내 지르코늄 전해정련공정에서 삼불화알루미늄의 효과 연구

Chang Hwa Lee[1,*], Deok Yoon Kang[1,2], Sung-Jai Lee[1], and Jong-Hyeon Lee[2]
[1]*Korea Atomic Energy Research Institute, 111, Daedeok-daero 989beon-gil, Yuseong-gu, Daejeon, Republic of Korea*
[2]*Chungnam National University, 99, Daehak-ro, Yuseong-gu, Daejeon, Republic of Korea*

이창화[1,*], 강덕윤[1,2], 이성재[1], 이종현[2]
[1]*한국원자력연구원, 대전광역시 유성구 대덕대로989번길 111*
[2]*충남대학교, 대전광역시 유성구 대학로 99*

(Received June 19, 2019 / Revised June 21, 2019 / Approved June 24, 2019)

Zr electrorefining is demonstrated herein using Zirlo tubes in a chloride-fluoride mixed molten salt in the presence of AlF_3. Cyclic voltammetry reveals a monotonic shift in the onset of metal reduction kinetics towards positive potential and an increase in intensity of the additional peaks associated with Zr-Al alloy formation with increasing AlF_3 concentration. Unlike the galvanostatic deposition mode, a radial plate-type Zr growth is evident at the top surface of the salt during Zr electrorefining at a constant potential of −1.2 V. The diameter of the plate-type Zr deposit gradually increases with increasing AlF_3 concentration. Scanning electron microscopy–energy-dispersive X-ray spectroscopy (SEM-EDX) and X-ray photoelectron spectroscopy (XPS) analyses for the plate-type Zr deposit show that trace amount of Al is incorporated as Zr-Al alloys with different chemical compositions between the top and bottom surface of the deposit. Addition of AlF_3 is effective in lowering the residual salt content in the deposit and in improving the current efficiency for Zr recovery.

Keywords: Zirconium recovery, Electrorefining, Cladding hull, Molten salt, Zr-Al alloys

*Corresponding Author.
Chang Hwa Lee, Korea Atomic Energy Research Institute, E-mail: chwalee@kaeri.re.kr, Tel: +82-42-868-4477

ORCID

Chang Hwa Lee	http://orcid.org/0000-0002-4624-5738	Deok Yoon Kang	http://orcid.org/0000-0003-1221-587X
Sung-Jai Lee	http://orcid.org/0000-0001-7639-1210	Jong-Hyeon Lee	http://orcid.org/0000-0003-3193-9128

삼불화알루미늄(AlF_3)이 포함된 염화물-불화물 혼합 용융염에서 ZIRLO 튜브를 이용한 지르코늄 전해정련공정을 실증하였다. 순환 전압전류실험 결과, AlF_3의 농도가 증가함에 따라 금속환원의 개시 전위가 일정하게 증가하고 지르코늄-알루미늄 합금형성과 관련된 추가적인 peak의 크기가 점차 증가하는 것으로 나타났다. 전류조절 전착법과 달리, −1.2 V의 일정전위에서 수행한 지르코늄 전해정련에서 방사형 판 구조의 지르코늄 성장이 염의 상단 표면에서 확연하게 나타났으며, 전착물 지름의 크기는 AlF_3의 농도에 따라 점차 증가하는 것으로 나타났다. 주사전자현미경(SEM)과 에너지 분산 X선 분광기(EDX)와 X선 광전자 분광기(XPS)를 이용하여 판 구조의 지르코늄 전착물을 분석한 결과, 극미량의 알루미늄이 지르코늄-알루미늄 합금 형태로 존재하며, 전착물의 상단과 하단 간에 서로 다른 화학성분구조를 갖는 것으로 나타났다. AlF_3의 첨가는 전착물 내 잔류염 양을 줄이고, 지르코늄 회수를 위한 전류효율을 향상시키는 데 효과적인 것으로 나타났다.

중심단어: 지르코늄 회수, 전해정련, 피복관, 용융염, 지르코늄-알루미늄 합금

1. Introduction

Pyroprocessing is a highly non-proliferate technology that can be used to reduce the amount of high-level waste and enhance the utilization of energy sources by separating highly radioactive fission products and recycling uranium (U) and transuranic (TRU) elements from used nuclear fuel (UNF) using high-temperature molten salt electrochemistry [1, 2]. In head-end pyroprocessing, cladding hulls and hardware are supposedly generated as metal wastes for the treatment of pressurized light-water reactors (PWRs). Among the metal wastes, cladding hull wastes are composed of Zr-based alloys and is produced at the rate of ~2.6 tons per 10 tons of UNF [3]. Particularly, since trace amount of UNF may remain inside the cladding tubes after decladding, the cladding hull waste is assumed to be an intermediate-level waste (ILW) in the domestic regulation for radioactive wastes or a “greater than class C” (GTCC) waste, based on the U.S. regulations [4, 5]. Therefore, recycling Zr, which is the main component of cladding hull, is substantially advantageous for the reduction of metal waste.

Representative Zr recovery processes include a chlorination reaction using Cl_2 gas [6] and electrorefining using molten salt electrochemistry [3, 7]. The electrorefining process involves the deposition of highly pure Zr on cathode by applying a current or voltage between the anode basket (filled with cladding wastes) and cathode in high-temperature molten salt electrolytes. Although the chlorination reaction effectively processes a large quantity of Zr-based cladding hull wastes due to its fast reaction kinetics, toxic Cl_2 gas is used, and an additional Kroll process is required to covert $ZrCl_4$ to metallic Zr for further applications. On the other hand, the electrorefining process is advantageous for directly recovering Zr in a metallic form. However, the electrochemical reaction mechanism of Zr is complicated and the amount of residual salt in the Zr deposit is considerably high because Zr is recovered as a powder-type deposit in chloride-based molten salts. To resolve this issue, many researchers have studied fluoride-based molten salts like FLiNaK for Zr recovery and acquired coherent Zr deposits [8-10]. However, fluoride-based salts require higher operation temperatures ranging from 700℃ to 900℃ due to their higher melting points and their applications are limited to materials such as crucibles, electrodes, etc.

In a previous study, we examined a chloride-fluoride mixed salt for overcoming the disadvantages of all-chloride and all-fluoride salts [11]. Cyclic voltammograms showed that Zr complex ions of various oxidation states are stabilized as Zr^{4+} in LiCl-KCl-$ZrCl_4$ salts by the addition of the fluoride compound, LiF, which strongly supports the substitution of complexing ions. In addition, through

the electrorefining process for Zirlo tubes, better-quality dendrite-type Zr deposit was grown with significant reduction in residual salt content in the mixed chloride-fluoride salt. There has been limited research on the effect of additives on the electrodeposition of Zr for improving its morphology in molten salts. G. W. Mellors et al. examined purified ZrO_2, SiO_2, K_2SiF_6, and KBF_4 in chloride-fluoride mixed salt baths or all-fluoride salt baths and found that the addition of KBF_4 and Al_2O_3 produced Zr alloys as smooth coherent plates [10].

Herein we investigate the effect of AlF_3 addition on the morphological feature of Zr deposits during Zr electrorefining using chloride-fluoride mixed salts. Particularly, a consecutive process has been suggested for the enhancement of recovery yield of Zr.

2. Experimental

The base electrolyte used herein for Zr electrorefining was a chloride-fluoride mixed salt, consisting of anhydrous LiCl-KCl eutectic (99.99wt% purity, Sigma-Aldrich), 0.84 M LiF, and 0.07 M $ZrCl_4$ as an initiator. The effect of adding AlF_3 over the concentration range 0~38.6 mM in the mixed salt on Zr electrorefining was investigated. All the experiments were performed in an Ar-purging glove box where oxygen and moisture are maintained under 5 ppm. Cyclic voltammetry and chronoamperometry were performed using a potentiostat/galvanostat (BioLogics Model SP-150), which has a three-electrode cell including a 30 mm-long tungsten wire (1Ø) shielded within an alumina tube (3Ø) as the working electrode, a Zr rod or a half-cut Zirlo tube as the counter electrode, and a Ag/AgCl reference electrode to examine the effect of AlF_3 addition in LiCl-KCl-LiF-$ZrCl_4$ salt. The reference electrode was made by inserting a Ag wire in a 6Ø mullite tube partially filled with LiCl-KCl-1wt% AgCl. The operating temperature was fixed at 600℃ and the experiments were performed under a quiescent condition.

Quantitative chemical analysis of the Zr deposit was performed using inductively coupled plasm-atomic emission spectroscopy (ICP-AES) and ion chromatography (IC). Field-emission scanning electron microscopy (FESEM, Hitachi SU8010) and energy-dispersive X-ray analysis (EDX) were used to examine the microstructure of the electrorefined Zr deposit surface and its compositional distribution, respectively. X-ray diffraction (XRD, Bruker D8 Advance, Cu Kα = 1.5418 Å) was used to examine the crystallographic texture of the Zr deposit in the presence of AlF_3. In addition, X-ray photoelectron spectroscopy (XPS, Kratos AXIS Nova) was employed for chemical analysis of the electrorefined Zr surface. Monochromated Al Kα (1486.69 eV) was used to collect the spectra at an angle of 0° between the sample surface normal and the analyzer lens. A pass energy of 20 eV and step size of 0.1 eV were used for the high-resolution region scans. The binding energy scale was referenced with respect to C 1s at 284.6 eV.

3. Results and Discussion

Figure 1a shows the cyclic voltammetric curves for Zr reduction/oxidation in the presence of various concentrations of AlF_3 LiCl-KCl-LiF-$ZrCl_4$ salt at 600℃. In the absence of AlF_3, unlike the chloride-based salt in which a multi-step reduction of Zr ions is involved [7, 12, 13], a single-step reduction of Zr is evident at about −1.15 V for the chloride-fluoride mixed salt, attributed to a complexation of Zr ions with F ions as follows [14].

$$[ZrF_6]^{2-} + 4e^- \rightarrow Zr + 6F^- \quad (1)$$

With increasing AlF_3 concentration, additional shoulder peaks in the cathodic scans become relevant from about −1.26 V for 3.8 mM AlF_3 and shift slightly to −1.22 V and −1.2 V for 15.4 mM and 38.6 mM AlF_3, respectively, which should be associated with the reduction of Zr-Al alloys. For higher concentration of AlF_3, the peak potential approaches

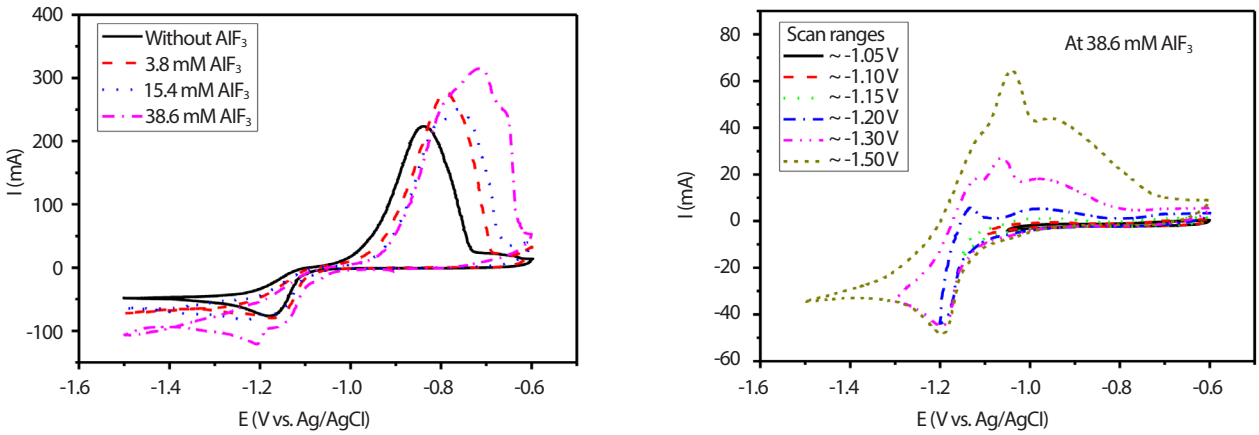

(a) (b)

Fig. 1. Cyclic voltammetric curves in the presence of various concentrations of AlF_3 in LiCl-KCl-LiF-$ZrCl_4$ salt at 600℃. W wire and Zr rod were used as the working and counter electrodes, respectively. The scan rate was fixed at 50 $mV \cdot s^{-1}$.

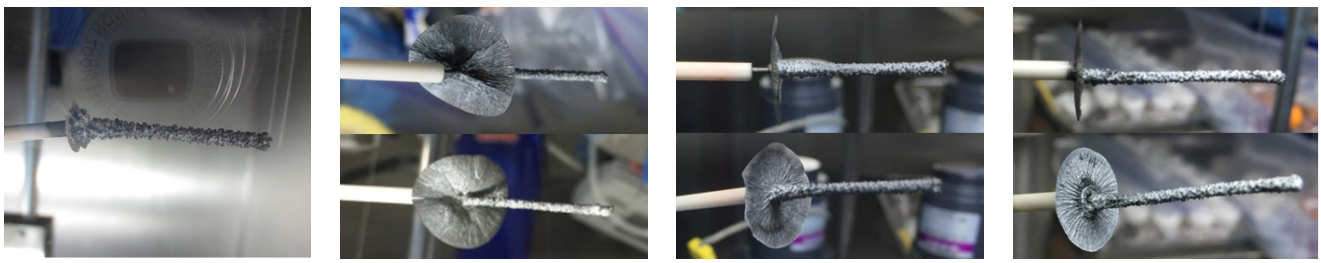

(a) (b) (c) (d)

Fig. 2. Photographic images of Zr deposits grown at various concentrations of AlF_3 in LiCl-KCl-0.84 M LiF-0.07 M $ZrCl_4$ at 600℃: (a) 0 (cited from Fig. 4b of reference [11]), (b) 3.8 mM, (c) 15.4 mM, and (d) 38.6 mM AlF_3. W wire and Zr rod (Zirlo tube as an anode for (a)) were used as the working and counter electrodes, respectively. The total electric charges for electrorefining process were −1,365 A·s for (a) and −540 A·s for (b), (c), and (d).

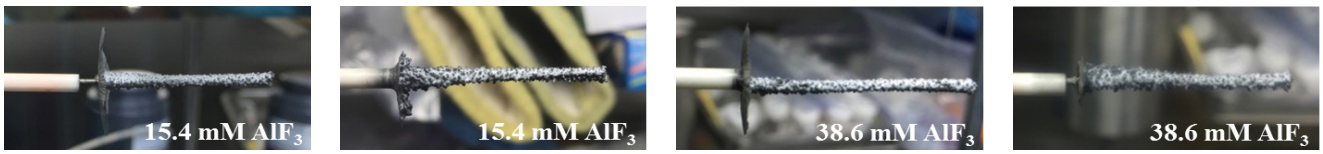

(a) (b) (c) (d)

Fig. 3. Photographic images of Zr deposits grown under (a, c) a constant-potential mode at −1.2 V and (b, d) a constant-current mode at −50 mA for the same electrical charge of −540 A·s. The AlF_3 concentrations were (a, b) 15.4 mA and (c, d) 38.6 mA in LiCl-KCl-0.84 M LiF-0.07 M $ZrCl_4$.

the reduction peak of Al (Fig. 1b). The formation of Zr-Al can also be evidenced from the peak shift for the oxidation of Zr at about −0.84 V and the appearance of additional peaks at a less negative potential regime between −0.75 V and −0.65 V. The Zr-Al alloy is known as a line compound formed in a specific chemical ratio according to the concentration of each component at a certain temperature [15]. Therefore, the peak shifts for the reduction and

oxidation of Zr and Al, depending on the concentration of AlF_3, can be analogized as the formation of Zr-Al alloys of different stoichiometries.

Zr electrorefining was performed at a constant potential of −1.2 V in the presence of various AlF_3 concentrations to examine the morphologies of Zr deposits (Fig. 2). To exclude the effect of area-dependent growth of Zr at a constant potential, the processing time was controlled by the same amount of electric charge (−540 A·s). For comparison, Zr deposit electrorefined from a Zirlo tube without AlF_3 in a previous study is displayed in Fig. 2a [11]. Although the total charge was less than a half of that for the AlF_3-free salt, a plate-like Zr deposit with a diameter of ~20 mm is evident in the presence of AlF_3, formed at the salt interface with a limited amount of deposit on the rest of the W rod.

Dependency of the growth mode was examined by applying a constant potential and current, as shown in Fig. 3. The morphologies of the Zr deposit for 15.4 mM and 38.6 mM AlF_3 were compared and the total electric charge passed during the electrorefining process was fixed at −540 A·s for both modes. For electrorefining at a constant current of −50 mA, thicker Zr deposits were formed on the W rods, with only small radial deposits at the salt interface due to a relatively homogenous deposition of Zr on the W rod. This is because the electrode potential is assumed to be become less negative towards the reduction of pure Zr, thereby forming relatively Zr-rich Zr-Al alloys with increasing electrode surface area during deposition. On the other hand, at a constant potential of −1.2 V, where Zr is deposited with a relatively higher Al content (Al-rich Zr-Al alloys), larger currents over −50 mA were passed (not shown) and the current continued to increase with expansion of surface area.

The amount of residual salt in the as-deposited Zr product recovered from the all-chloride salt reaches almost 90% because of the powder-type morphological feature. The residual salt content and current efficiency were compared for various molten salt electrolytes by removing the residual salt using vacuum distillation at 900℃ for 2 h, as shown in Table 1. The current efficiency was estimated with the ratio of actual mass of Zr deposit measured after distillation to the equivalent mass (W_{eq}) calculated from the total electric charge passed through the experimental setup, according to the following equation,

$$W_{eq} = \frac{Q_{tot} \times M_{Zr}}{nF} \quad (2)$$

where, Q_{tot} is the total charge, M_{Zr} is the molar mass of Zr, n is the valency of Zr ions, and F is the Faraday constant (96,485 C·mol^{-1}). The addition of LiF significantly reduced the residual salt content from 92% to 68% of the total amount of Zr deposit by changing the morphological feature from powder to dendritic. Even more reduction

Table 1. Residual salt contents in Zr deposits electrorefined in various molten salts

Molten salts	Residual salt contents (%)	Current efficiency (%)
LiCl-KCl-$ZrCl_4$	92	-
LiCl-KCl-$ZrCl_4$-LiF	68	57.1
LiCl-KCl-$ZrCl_4$-LiF-3.8 mM AlF_3	60	88.3
LiCl-KCl-$ZrCl_4$-LiF-15.4 mM AlF_3	64	77.3
LiCl-KCl-$ZrCl_4$-LiF-38.6 mM AlF_3	52	73.4

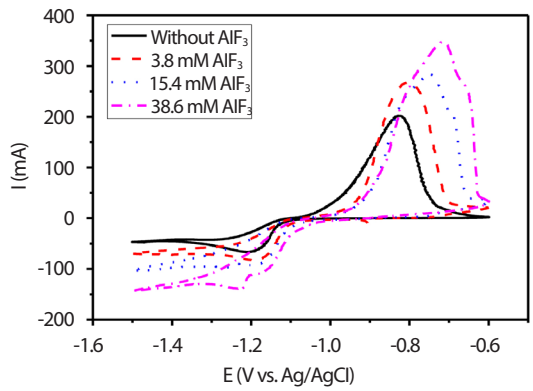

Fig. 4. Cyclic voltammetric curves in the presence of various concentrations of AlF_3 LiCl-KCl-LiF-$ZrCl_4$ salt at 600℃. W wire and Zirlo tube were used as the working and counter electrodes, respectively. The scan rate was fixed at 50 mV·s^{-1}.

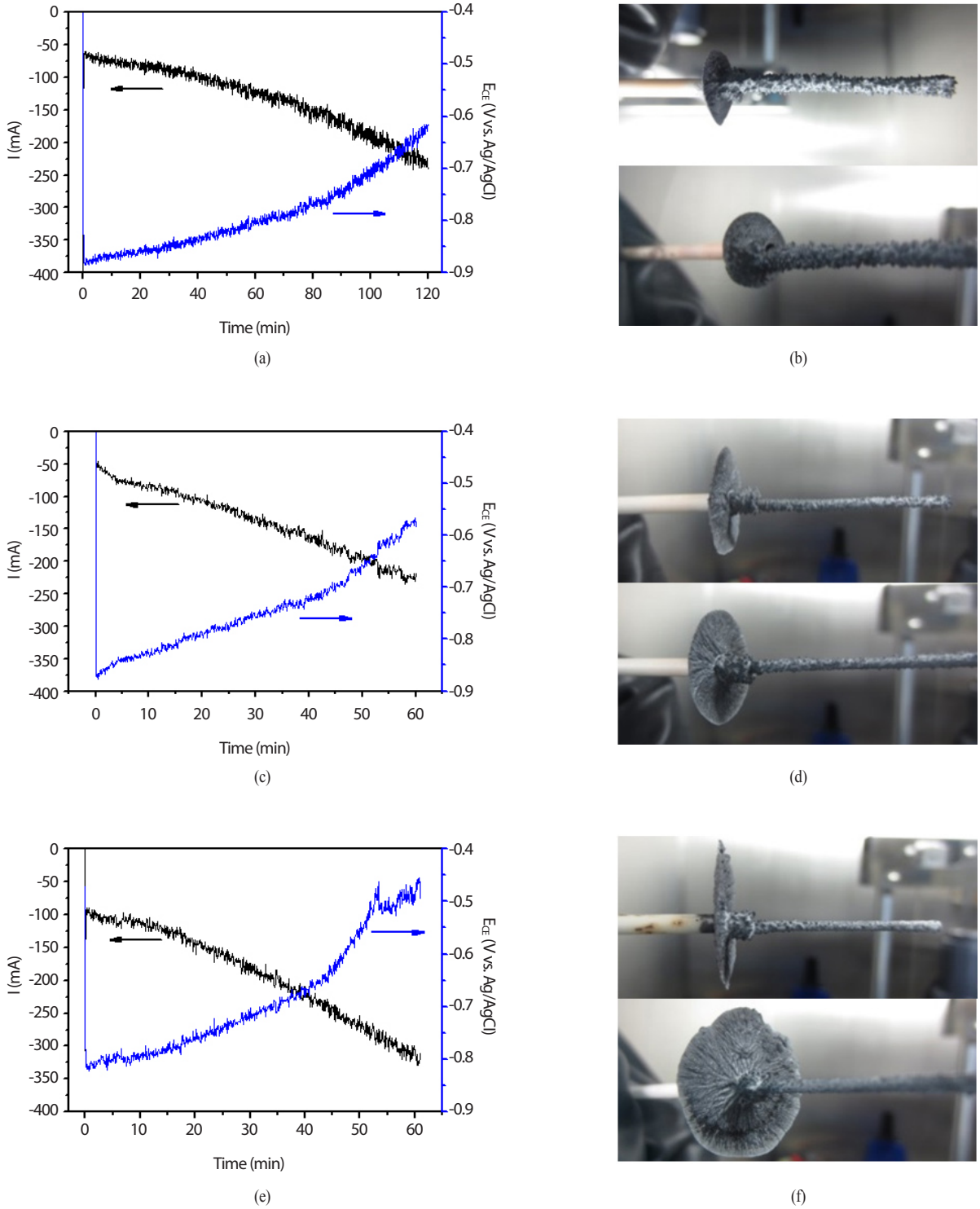

Fig. 5. Chronoamperometry results for Zr electrorefining and the corresponding photographic images of Zr deposits grown at various concentrations of AlF_3 LiCl-KCl-0.84 M LiF-0.07 M $ZrCl_4$ at 600℃; (a, b) 3.8 mM, (c, d) 15.4 mM, and (e, f) 38.6 mM AlF_3. W wire and Zirlo tube were used as the working and counter electrodes, respectively.

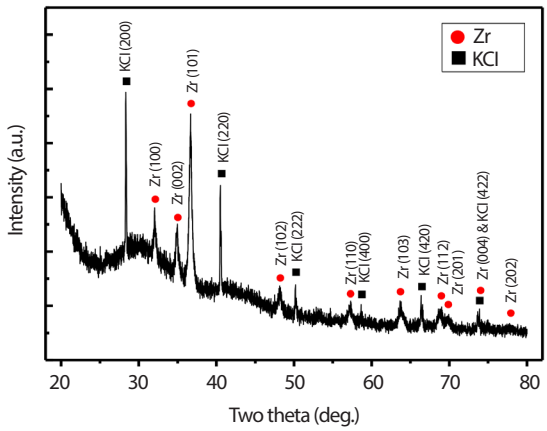

Fig. 6. XRD pattern for the surface of Zr deposit grown for 1 h at −1.2 V vs. Ag/AgCl in LiCl-KCl-0.84 M LiF-0.07 M $ZrCl_4$-15.4 mM AlF_3 salt. W wire and Zirlo tube were used as the working and counter electrodes, respectively.

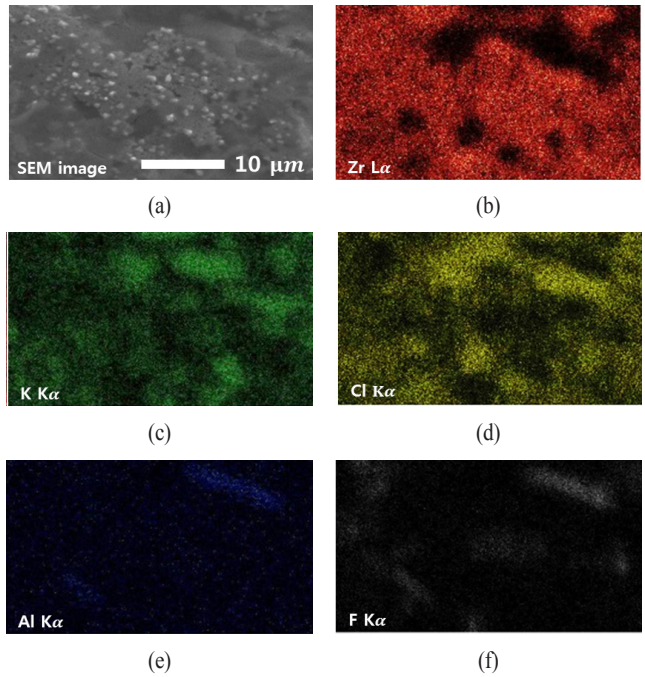

Fig. 7. SEM-EDX mapping images for the surface of Zr deposit grown for 1 h at −1.2 V vs. Ag/AgCl in LiCl-KCl-0.84 M LiF-0.07 M $ZrCl_4$-15.4 mM AlF_3 salt. W wire and Zirlo tube were used as the working and counter electrodes, respectively.

of the salt down to 50% was confirmed by the addition of AlF_3 due to the formation of plate-like deposits. The current efficiency was also enhanced from 57.1% for the AlF_3-free case to 88.3% for molten salt with 3.8 mM AlF_3.

Identical experiments were performed using a Zirlo tube-cut specimen as an anode to simulate the treatment of cladding hull waste. Figure 4 shows the cyclic voltammetric curves in the presence of various AlF_3 concentrations in LiCl-KCl-$ZrCl_4$-LiF salt. The voltammetric responses depending on the AlF_3 concentration for Zr rod are similar to those for Zirlo tubes, the onset and the peak potentials for Zr rod being only slightly greater than those for Zirlo. This may be related to the almost similar composition of Zirlo, i.e. Zr alloyed with only about 1wt% of Nb, 1wt% Sn, and 0.1wt% of Fe, whose electrochemical behavior should be analogous to that of pure Zr. Zr electrorefining experiments were carried out by applying a constant potential of 1.2 V, at which Al can be co-deposited with Zr in the respective molten salt electrolyte containing various AlF_3 concentrations (Fig. 5). The current transient becomes more negative faster for higher AlF_3 concentrations and the anodic potential increases correspondingly. In terms of the morphological features, the size of the radial metallic plate at the top of the salt interface gradually increases, while the diameter of the deposit on the rod decreases with increasing AlF_3 concentration.

To characterize the plate-type deposit formed at the top surface of the salt, the deposit grown at 15.4 mM AlF_3 was subjected to XRD analysis (Fig. 6). The specimen was simply rinsed with ethanol to remove the incorporated salt and placed in an XRD holder with an air-tight polymer seal for residual salt, which consequently produced the higher background signal at lower 2θ values. However, metallic Zr peaks are evident, unlike the diffraction patterns of Zr deposit grown in a chloride-based salt, which exhibited strong Zr oxide and weak Zr metal peaks [7]. Due to the solubility difference between LiCl and KCl in ethanol, only KCl peaks are observed for the salt composition [16]. To confirm the existence and distribution of Al in the Zr deposit, SEM-EDX compositional mapping analysis was performed for the top surface of the same specimen (Fig. 7).

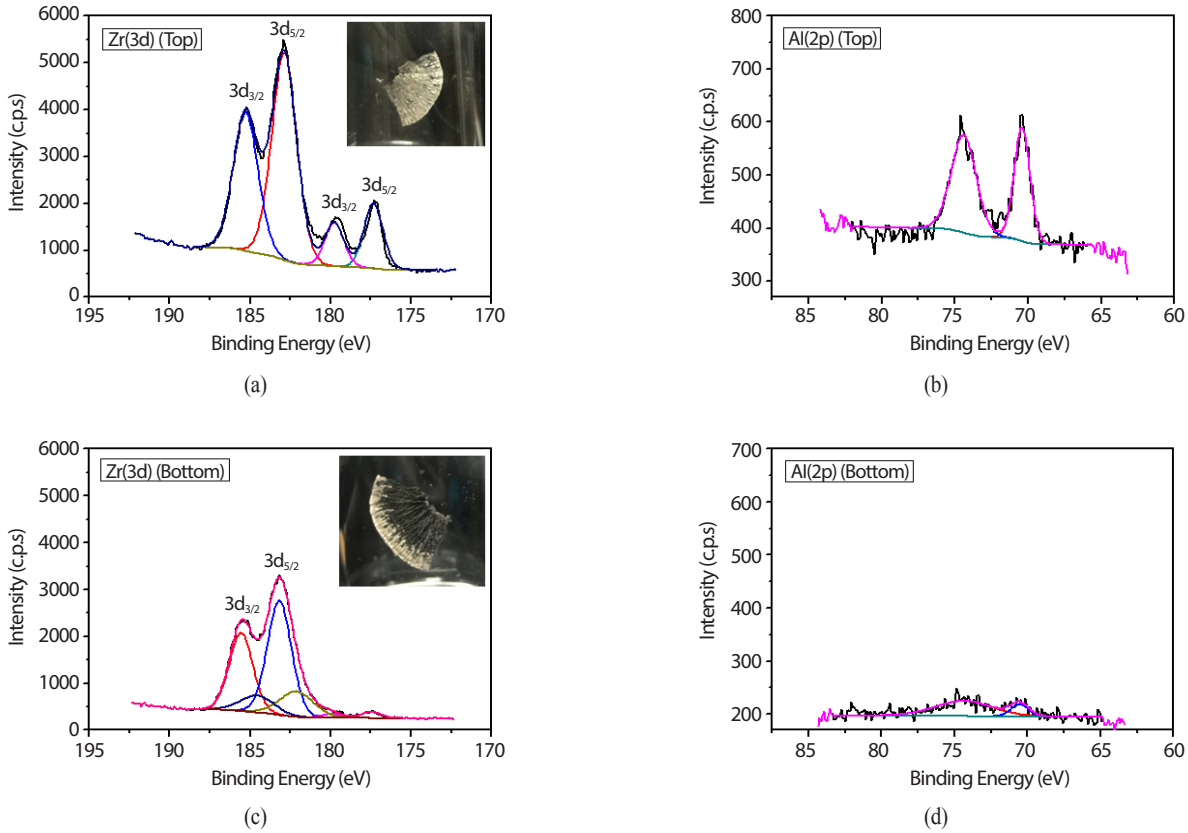

Fig. 8. XPS spectra of Zr(3d) and Al(2p) for the (a, b) top and (c, d) bottom surfaces of the Zr deposit grown for 1 h at −1.2 V vs. Ag/AgCl in LiCl-KCl-0.84 M LiF-0.07 M $ZrCl_4$-15.4 mM AlF_3 salt. W wire and Zirlo tube were used as the working and counter electrodes, respectively. The inset photographs show the actual samples analyzed by XPS.

The major X-ray signals emitted from the surface were due to Zr Lα and Cl Kα, corresponding to the deposit and the residual salt, respectively. A faint signal of Al Kα, which could also be attributed to the salt component from the residual salt, is shown to have uniform distribution over the surface. Evenly distributed Al signal supports the fact that the added Al was not locally reduced or extracted.

The plate-type Zr product formed at the salt interface appears to have different colors between the top and bottom surface of the product. XPS was utilized to examine the difference in chemical composition between the top and bottom surfaces (Fig. 8). After the deconvolution of the XPS spectra, the more silvery top surface of the deposit, electrorefined in the presence of 15.4 mM AlF_3, yields well defined $Zr(3d_{5/2})$ and Al(2p) peaks corresponding to ZrO_2 at 182.8 eV and Al oxide at 74.4 eV, respectively, which were natively formed during sample preparation. The additional $Zr(3d_{5/2})$ and Al(2p) peaks at 177.7 eV and 70.4 eV, respectively, are thought to be associated with slightly shifted metallic forms and/or Zr-Al alloys. In comparison with the top surface, the intensity of photoelectron for the bottom surface was lower due to the scattering effect by the higher surface roughness, as indicated by its darker color. The $Zr(3d_{5/2})$ peaks that are split into ZrO_2 (183.1 eV) and Zr sub-oxide (182.0 eV) and Al(2p) peaks, corresponding to almost the same positions, are evidently attributed to relatively reduced Al and Zr that might be alloyed with Al at lower binding energies. From the measured intensities of

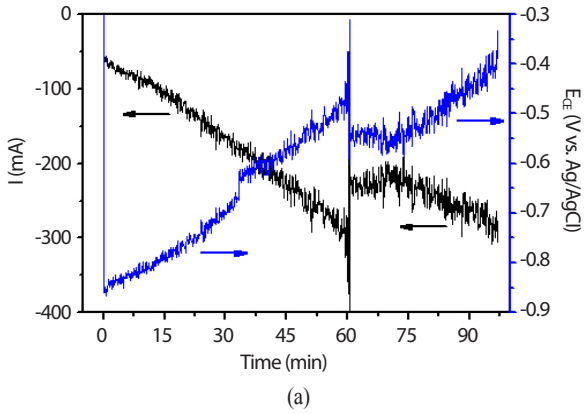

(a)

(b)

Fig. 9. (a) Chronoamperometry results obtained with an intermittent break for a two-step Zr recovery process and (b) photographic image of the Zr product.

Zr(3d) and Al(2p) spectra, the approximate atomic ratios (N_{Zr}/N_{Al}) for the top and bottom surfaces were derived as 2.46 and 5.47, respectively, based on the following equation,

$$\frac{I_{Zr}}{I_{Al}} \approx \frac{N_{Zr}\sigma_{Zr}\lambda_{Zr}}{N_{Al}\sigma_{Al}\lambda_{Al}} \text{ and } \lambda_i\,(\text{Å}) = 9.0 + 0.022KE_i\,(eV) \quad (3)$$

where I is the area intensity of photoelectron peak, σ is the photoelectron cross-section [Scofield factors [17], $\sigma_{Al} = 0.234$, $\sigma_{Zr} = 1.546$], λ is the mean free path [$\lambda_{Al} = 40.10$ Å, $\lambda_{Zr} = 37.77$ Å], and KE the kinetic energy of the respective photoelectrons. The stoichiometries do not exactly match those of the Zr-Al compounds in the phase diagram because metallic Zr can also be deposited with Zr-Al alloys; however, the Zr-Al alloys are approximately positioned between Zr_2Al and Zr. Particularly, relatively Al-rich and Zr-rich Zr-Al alloys are detected at the top and bottom surfaces, respectively, of the plate-type deposit. This shows that lighter Al that is reduced and floats around the cathode at temperatures slightly lower than its melting point ($T_{m,\,Al} = 660$℃) can form a seed of radial shape for heterogenous growth of Zr and Zr-Al alloys at the salt interface.

A consecutive Zr recovery process in the plate-type deposit at the salt surface was confirmed by repeating the chronoamperometry experiment with an intermittent break (Fig. 9). After applying a potential of −1.2 V for 60 min in the same LiCl-KCl-$ZrCl_4$-LiF electrolyte with 15.4 mM AlF_3, the W cathode was lifted up by ~10 mm during the intermittent break and chronoamperometry was continued at the same applied voltage of −1.2 V for 37 min (Fig. 9a). An instant charging current was flown up to −400 mA for few subseconds and the cathodic current began from about −220 mA, lower than the current before the break because the electrode surface area contact with the salt decreased, followed by a gradual increase in current with time. As observed in Fig. 9b, the morphology of the Zr deposit reveals two radial plates at intervals of ~10 mm from the top of the W cathode that meets the alumina shield. At the same time, thick dendritic Zr deposits were formed on the peripheral region of the W rod.

4. Conclusion

Powder-type Zr morphology is the main obstacle to recovering Zr using electrorefining in chloride-based molten salts with high recovery yield. Herein we investigated the effect of adding AlF_3 on Zr electrorefining in chloride-fluoride mixed molten salt, LiCl-KCl-$ZrCl_4$-LiF, at 600℃. Voltammetric experiments in the presence of various concentrations of AlF_3 revealed that a similar monotonic shift of Zr reduction peaks and additional peaks occurred for both Zr rods and Zirlo tubes as anodes, attributed to the formation of Zr-Al alloys. During Zr electrorefining

at a constant potential of −1.2 V, AlF_3 addition led to a preferential recovery of Zr around the top of electrode adjacent to the salt surface by forming a radial plate-type Zr deposit, whose size was increased with increasing AlF_3 concentration. The amount of residual salt in the deposit was significantly decreased in the chloride-fluoride mixed salts both in the presence and the absence of AlF_3, compared to the all-chloride based salt. The calculated current efficiency was increased by the addition of AlF_3 in the chloride-fluoride mixed salt. Surface analysis of the radial deposit using XPS identified relatively higher Al content on the top surface than on the bottom for the recovered Zr-Al alloys, which supports the assumption that the floating Al acts as a seed for the heterogeneous growth of Zr deposit at the salt surface. The Zr recovery yield should be enhanced in the chloride-fluoride mixed salt by using AlF_3 as an additive at a relatively low temperature of 600℃.

Acknowledgement

This work was supported by the National Research Foundation of Korea (NRF) grant, funded by the Korean Ministry of Science and ICT (MSIT) [grant number 2017M 2A8A5015079].

REFERENCES

[1] J.P. Ackerman, "Chemical Basis for Pyrochemical Reprocessing of Nuclear Fuel", Ind. Eng. Chem. Res., 30, 141-145 (1991).

[2] J.J. Laidler, J.E. Battles, W.E. Miller, J.P. Ackerman, and E.L. Carls, "Development of Pyroprocessing Technology", Prog. Nucl. Energ., 31, 131-140 (1997).

[3] C.H. Lee, M.K. Jeon, C.M. Heo, Y.L. Lee, K.H. Kang, and G.I. Park, "Effect of Zr Oxide on the Electrochemical Dissolution of Zircaloy-4 Cladding Tubes", J. Electrochem. Soc., 159, E171-E176 (2012).

[4] T.S. Rudisill, "Decontamination of Zircaloy Cladding Hulls from Spent Nuclear Fuel", J. Nucl. Mater., 385, 193-195 (2009).

[5] U.S. Japan Joint Nuclear Energy Action Plan Waste Management Working Group Phase I Report, U.S. Department of Energy, FCR&D-USED-2010-000051 (2010).

[6] M.K. Jeon, K.H. Kang, G.I. Park, and Y.S. Lee, "Chlorination Reaction Behavior of Zircaloy-4 Hulls: Experimental and Theoretical Approaches", J. Radioanal. Nucl. Chem., 292, 513-517 (2012).

[7] C.H. Lee, K.H. Kang, M.K. Jeon, C.M. Heo, and Y.L. Lee, "Electrorefining of Zirconium from Zircaloy-4 Cladding Hulls in LiCl-KCl Molten Salts", J. Electrochem. Soc., 159, D463-D468 (2012).

[8] G.J. Kipouros and S.N. Flengas, "Electrorefining of Zirconium Metal in Alkali Chloride and Alkali Fluoride Fused Electrolytes", J. Electrochem. Soc., 132, 1087-1098 (1985).

[9] J.A. Gurklis, J.G. Beach, and C.L. Faust, Report No. BMI-781, Battelle Memorial Institute, Columbus, Ohio (1952).

[10] G.W. Mellors and S. Senderoff, "The Electrodeposition of Coherent Deposits of Refractory Metal III. Zirconium", J. Electrochem. Soc., 113, 60-66 (1966).

[11] C.H. Lee, D.Y. Kang, M.K. Jeon, K.H. Kang, S.-W. Paek, D.-H. Ahn, and K.-T. Park, "Addition Effect of Fluoride Compounds for Zr Electrorefining in LiCl-KCl Molten Salts", Int. J. Electrochem. Sci., 11, 566-576 (2016).

[12] S. Ghosh, S. Vandarkuzhali, N. Gogoi, P. Venkatesh, G. Seenivasan, B.P. Reddy, and K. Nagarajan, "Anodic Dissolution of U, Zr and U-Zr Alloy and Convolution Voltammetry of $Zr^{4+}|Zr^{2+}$ Couple in Molten LiCl-KCl Eutectic", Electrochim. Acta, 56, 8204-8218 (2011).

[13] J. Park, S. Choi, S. Sohn, and I.S. Hwang, "Cyclic Voltammetry on Zr, Sn, Fe, Cr and Co in LiCl-KCl Salts at 500℃ for Electrorefining of Irradiated Zircaloy-4 Cladding", J. Electrochem. Soc., 164, D744-D751 (2017).

[14] A. Girginov, T.Z. Tzvetkoff, and M. Bojinov, "Electrodeposition of Refractory Metals (Ti, Zr, Nb, Ta) from Molten Salt Electrolytes", J. Appl. Electrochem., 25, 993-1003 (1995).

[15] M. Alatalo, M. Weinert, and R.E. Watson, "Stability of Zr-Al Alloys", Phys. Rev. B, 57, R2009 (1998).

[16] M. Li, D. Constantinescu, L. Wang, A. Mohs, and J. Gmehling, "Solubilities of NaCl, KCl, LiCl, and LiBr in Methanol, Ethanol, Acetone, and Mixed Solvents and Correlation Using the LIQUAC Model", Ind. Eng. Chem. Res., 49, 4981-4988 (2010).

[17] J.H. Scofield, "Hartree-Slater Subshell Photoionization Cross-sections at 1254 and 1487 eV", J. Electron Spectrosc. Relat. Phenom., 8, 129-137 (1976).